Convective instabilities induced by an exothermic autocatalytic chemical reaction

Bice S. Martincigh
Department of Chemistry and Applied Chemistry, University of Natal, King George V Avenue, 4001 Durban, South Africa

Reuben H. Simoyi
Center for Nonlinear Science and the Chemistry Department, West Virginia University, P.O. Box 6045, Morgantown, West Virginia 26506-6045

(Received 3 February 1995)

A bistable or excitable exothermic chemical reaction can produce a traveling front of chemical reactivity upon being triggered. The dynamics of the wave propagation are greatly influenced by the amount of heat generated at the wave front, which in turn is a function of (nonlinear) reaction kinetics, enthalpy change, and extent of reaction. The chemical reaction investigated here has shown complex propagative patterns, including accelerating big waves, convective rolls, double-diffusive convection, and spatiotemporal patterns. A model devised to explain the patterns involves a laterally heated fluid layer in which the basic flow loses stability in the form of hydrothermal waves. Wave motion is preceded by a global circulation between the hot and cold regions, with the velocity being proportional to the lateral temperature gradient. In this highly exothermic reaction the spatiotemporal patterns can be explained by a stability analysis of the Bénard-Marangoni convection with lateral heating.

PACS number(s): 47.70.Fw, 47.20.Dr, 82.20.Mj

INTRODUCTION

To date, the fascinating problem of lateral instabilities in the form of traveling wave fronts and spatiotemporal pattern generation from unstirred chemical reaction solutions has been treated as a coupling between chemical diffusion and nonlinear kinetics [1,2]. Chemical waves have been described by [3]

$$\delta c/\delta t = D\nabla^2 c + f(c) , \tag{1}$$

where c is a vector of state variables, D is the matrix of diffusion coefficients, and $f(c)$ is a function representing nonlinear chemical kinetics. Our recent work finds that Eq. (1) is an oversimplification of a much more complex problem. The validity of Eq. (1) is very confining as it requires gelling for convection-free conditions [4]. Equation (1) has also been more effective in describing one- and two-dimensional projections (thin layers) [5] as the full three-dimensional problem is still too complex.

There is not yet a firm establishment of the mechanisms which drive propagating convection fronts [6]. An autocatalytic (bistable) exothermic chemical reaction can generate a propagating convective instability emanating from a point of initial perturbation. In such dissipative chemical systems, a spatially periodic structure can grow out of a homogeneous state when a critical parameter (e.g., the temperature gradient) exceeds a certain value [7]. In dilute reaction systems, most propagation studies have focused on the solute in terms of diffusivities and chemical kinetics. In this paper we propose that a more realistic model can be derived on the basis of hydrothermal waves.

The phenomenon of cellular convection when a horizontal fluid layer is heated from below was discovered by Bénard [8] and explained by Lord Rayleigh [9] on the basis of instabilities due to buoyancy resulting from the expansion of a heated fluid (Rayleigh-Bénard convection). Pearson [10] suggested that, if the upper surface of the fluid layer was free, then the Bénard cells could be produced by tractions arising from the variation of surface tension caused by the temperature changes. Thus Bénard cells could be formed by hydrothermal convection driven by surface tension (Marangoni convection). By neglecting gravity waves, Pearson's theory failed in many critical areas [11]. For example, Pearson's theory could not produce a critical driving parameter involving surface tension in shallow layers with deformable surfaces, and neither could it explain the bidirectional fluid transfer observed in the Bénard cells. Rayleigh's and Pearson's theories were combined by Nield to yield a new theory in which buoyancy and thermocapillary effects are coupled [12].

The importance of Marangoni convection as a cause of the instabilities is now well established. Marangoni convection is the only natural convection mechanism under weightlessness conditions [13]. Surface tension decreases with temperature in most liquids [14]. Any temperature gradient along the free surface will induce a flow from hot to cold. The Marangoni number M is generally accepted as a measure of thermocapillary forces [15]:

$$M = -(\delta\sigma/\delta T)\Delta T l/\eta\chi , \tag{2}$$

where $\delta\sigma/\delta T$ is the temperature coefficient of the surface tension σ, ΔT is the temperature difference along the surface, l the length of the surface, η the dynamic viscosity, and χ the thermal diffusivity.

The coupling of buoyancy effects and thermocapillary convection is known as the Bénard-Marangoni instability [16]. Buoyancy forces can be estimated by the Grashof number Gr [17]:

$$\mathrm{Gr} = -(\delta\rho/\delta T) g \Delta T d^3/\eta\nu \ , \quad (3)$$

where $\delta\rho/\delta T$ is the temperature coefficient of the density of the fluid ρ, g is the earth's gravity, d is the depth of the solution, and ν is the fluid's kinematic viscosity. A pure Marangoni convection system can be studied in very thin horizontal layers ($\mathrm{Gr}=0$ as $d\rightarrow 0$), and buoyancy forces can be studied exclusive of Marangoni convection in tall thin tubes ($M=0$ as $l\rightarrow 0$).

We report in this paper on the very interesting traveling wave dynamics and spatiotemporal patterns observed in a highly exothermic chemical reaction in which no attempt was made to control the temperature. The motivation of this work was to give an accurate estimation of the effects of reaction-diffusion mechanisms and convective (both Marangoni and Rayleigh-Bénard) mechanisms.

Chemistry of wave formation

The reaction system being studied is the oxidation of a series of thiocarbonyl-like compounds by chlorite [18]. The oxidation products are sulfate and a urea-type residue; e.g.,

$$R\mathrm{C}{=}\mathrm{S} + p\mathrm{ClO_2}^- + \mathrm{H_2O} \rightarrow \mathrm{SO_4}^{2-} + R\mathrm{C}{=}\mathrm{O} + p\mathrm{H}^+ + p\mathrm{Cl}^- \ , \quad (4)$$

where R could be one of $(\mathrm{H_2N})_2$ (thiourea), $(\mathrm{CH_3NH})(\mathrm{NH_2})$ (1-methyl-2-thiourea), or $(\mathrm{PhHN})(\mathrm{NHNH_2})$ (4-phenyl-3-thiosemicarbazide). These reactions present clock reaction characteristics in which initially there is a quiescent period with no activity in the reaction indicators. At the end of the induction period there is a sudden production of $\mathrm{SO_4}^{2-}$, $\mathrm{ClO_2}$, and H^+. The acid and $\mathrm{SO_4}^{2-}$ are formed simultaneously from the oxidation of the sulfonic acid intermediate [19]:

$$R\mathrm{CSO_3H} + 2\mathrm{H_2O} \rightarrow \mathrm{SO_4}^{2-} + R\mathrm{C}{=}O + 4H^+ + 2e^- \ . \quad (5)$$

The $\mathrm{ClO_2}$ is formed by an extraneous $\mathrm{ClO_2}^-$-HOCl reaction [20]:

$$2\mathrm{ClO_2}^- + \mathrm{HOCl} + \mathrm{H}^+ \rightarrow 2\mathrm{ClO_2} + \mathrm{Cl}^- + \mathrm{H_2O} \ . \quad (6)$$

HOCl is the autocatalytic species which controls the rates of reaction and wave propagation [21]. The mechanism for autocatalysis involves the reactive intermediate $\mathrm{Cl_2O_2}$ leading to quadratic autocatalysis [22]

$$\mathrm{ClO_2}^- + \mathrm{HOCl} + \mathrm{H}^+ \rightarrow \mathrm{Cl_2O_2} + \mathrm{H_2O} \quad (7)$$

followed by

$$\mathrm{Cl_2O_2} + 2e^- + 2\mathrm{H}^+ \rightarrow 2\mathrm{HOCl} \ . \quad (8)$$

Apart from H^+, $\mathrm{SO_4}^{2-}$, and $\mathrm{ClO_2}$, the most important product in terms of wave propagation is a large heat evolution. The heat generated is so high that the reaction of thiourea and chlorite has an enthalpy of reaction in excess of $-1\,000\ \mathrm{kJ\ mol^{-1}}$. Temperature changes at the reaction front can go as high as $\Delta T = 70\,^{\circ}\mathrm{C}$ depending upon initial reagent concentrations. In unbuffered solutions the production of H^+ can be used as an indicator for the position of the wave front. Other indicators used include $\mathrm{BaSO_4}$ precipitation and freshly prepared starch. Formation of $\mathrm{SO_4}^{2-}$ anywhere in the solution will be indicated by the formation of white $\mathrm{BaSO_4}$. This is the least invasive way to observe convective rolls and patterns at the wave front and in the reacted regions. The light reflected on the $\mathrm{BaSO_4}$ crystals can clearly indicate the direction of fluid flow at the surface and within the bulk of the solution. A pH indicator, meanwhile, can only indicate the position of the wave front, but will not be able to indicate fluid motion.

Earlier studies of these reactions had shown highly structured wave fronts with double-diffusive convection [23]. The propagation of the wave fronts, as well, has shown complex convective and spatial reaction patterns which could be deduced from the $\mathrm{BaSO_4}$ precipitation patterns [24].

EXPERIMENT

Stock solutions were prepared from the following reagents: thiourea (Fisher), sodium chlorite (Kodak), and barium chloride (Caledon Laboratories). The commercially available technical grade sodium chlorite varied in purity from 78% to 81%. The sodium chlorite was recrystallized from a water-ethanol mixture and standardized iodometrically [25]. No other agents required purification. The stock solutions were prepared fresh daily. Extra care was also given to the chlorite which was stored in dark Winchester bottles to avoid excessive exposure to light.

Reaction mixtures were prepared from these stock solutions to give a final thiourea concentration of $0.020M$, with the sodium chlorite concentration being maintained at (at least) twice the thiourea concentration to ensure the formation of exotic dynamics [23]. Barium chloride concentrations were kept at about $0.05M$. Thiourea and barium chloride were vigorously mixed in a beaker and the sodium chlorite was added last by means of a rapid delivery pipette. After complete mixing, the reaction solution was poured into the reaction vessel, allowed to settle, and then triggered.

The reactions were performed in Plexiglass vessels of various geometries and dimensions as detailed in Table I. The vessel geometries were chosen so as to assess interfa-

TABLE I. Geometries and dimensions of the Plexiglass reaction vessels used to observe the wave propagation behavior. The triangular vessel and rectangle (C) were used for the observation of convective tori formations. Rectangle (A) was used to evaluate the role of reaction vessel walls on the wave propagation [Figs. 3(a)–3(d)]. Rectangle (B) was used for the observation of the side view of the wave (Figs. 4, 7, and 8).

Reaction vessel geometry	Inner dimensions
Isosceles triangle	base length 7.4 cm side length 15 cm base angles 76° top angle 28°
Rectangle (A)	length 25.4 cm width 2.0 cm
Rectangle (B)	length 25.3 cm width 0.5 cm
Rectangle (C)	length 24.3 cm width 15.3 cm

cial effects and boundary conditions.

The thoroughly mixed reaction solution was poured into the respective vessel and the wave initiated by adding a drop of solution containing dilute chlorine dioxide [23]. The wave dynamics in each vessel were studied at three solution depths and at different positions of the initiation point.

Image analysis and wave dynamics

Video imaging experiments were useful for studying the wave velocities, the structure of the propagating wave front, and the spatiotemporal patterns. All experiments were recorded using a PULNIX TMC 74 color camera attached to a Sony PVM-1334Q RGB monitor and a Panasonic AG-1960 professional videocassette recorder. The videocassette recorder and the RGB monitor were also interfaced to a 486-type 33-MHz computer via a PCVision Plus frame grabber model PFGPlus-640-3-60 capable of storing a 640×480 square pixels image. Image analysis was via Bioscan Optimas version 4.02 computer software. The recorded experiments were played back on the videocassette and the desired frames captured and stored as TIFF (Tagged Image File Format) computer files. The velocities were measured using the motion analysis macro of the BIOSCAN software which uses Microsoft Excel 4.0 software for the statistical analysis. Further processing of the acquired images included noise and color filtering.

RESULTS

The results reported here were obtained with $BaCl_2$ as indicator. Different solution depths were used, but these can be put into three separate groups: (i) shallow layers, $d \leq 1.9$ mm, (ii) medium layers, $1.9 \leq d \leq 3.4$ mm, and (iii) deep layers, $d \geq 5.0$ mm.

General wave dynamics

The wave could be left to initiate on its own or initiated electrochemically. In most of our experiments the wave was initiated by adding a drop of reaction mixture containing $HOCl$-ClO_2. The point of initiation of the wave was very important. The wave could be initiated in the center of the reaction solution, along the reactor edge, or at the corner of the reaction vessel. When initiated from the edge of the reaction vessel, the wave (of $BaSO_4$ precipitate, H^+, and ClO_2) moves off from the point of initiation of periodic semicircle precipitation patterns which pulsate out from this point. In medium depths these periodic precipitation patterns can be maintained for abut 5–6 cycles before they are lost as convective back rolls commence, which interfere with the initial precipitation to give serpentine precipitation patterns [26]. In general, the convective back rolls move back towards the point of initiation. At first the back rolls are fairly small but they become longer and more forceful with time. The wave is made up of three distinct regions: a leading edge which is characterized by a region of faint precipitation, a convective region in which the solution levels are sliding against each other with the top layer going in the direction of wave propagation while the bottom layer contains a back flow, and a third region made up of serpentine precipitation patterns. Figure 1(a) shows a typical big wave in these convective systems.

A very interesting feature of this wave is that the leading edge of the wave is separated from the convective region by a line of very faint or null precipitation [Fig. 1(b)] [27]. When the precipitation in the main body of the wave attains a homogeneous appearance this faint line is lost and replaced by a much wider region which has a mottled appearance. Almost as soon as this is achieved the velocity of the main wave decreases and propagative motion at the sides of the vessel becomes faster than in the middle of the vessel. Generally the wave starts off fast and rapidly decelerates sometime into the reaction vessel [28]. In the very large rectangular vessels, in which the effects of vessel boundary on wave propagation are not strong, one can track separately the velocities of the leading edge and the start of the convective back flow. After the initial deceleration, the velocity of the leading edge attains an almost constant velocity. The velocity of the second front, however, is found to be oscilla-

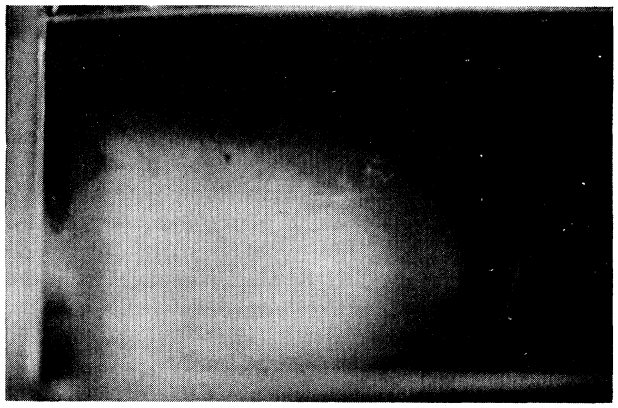

(a)

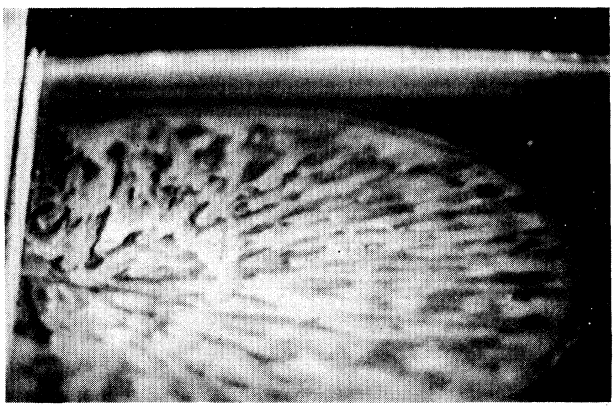

(b)

FIG. 1. (a) A typical wave observed in a large vessel (with no interference from the walls). Leading edge is clearly marked by faint precipitation; the next region has inhomogeneous $BaSO_4$ precipitate distribution. The width of the leading edge in this figure is 12 mm. (b) Close-up of the leading front which is separated from the rest of the wave by an annulus of null precipitation. The annulus shown here is 3 mm wide.

tory. Figure 2 shows the velocity variations of each front. The second front alternately accelerates and decelerates, although it never overtakes the leading front.

In the smaller rectangles, the wave starts off with a convex-shaped wave front, and when the wave decelerates the wave along the sides of the vessel overtakes the wave in the center of the vessel and reaches the end of the vessel first [29]. This almost has the appearance of two arms which then move along the facing edge of the vessel. Figures 3(a)–3(d) show this trend. If the main wave has reached the facing edge these "arms" meet with it; otherwise the two arms themselves meet and then move back towards the leading front of the main wave.

Of interest was the interaction between waves. Two waves were initiated from different sides of a long rectangular narrow vessel and allowed to diffuse towards each other. There seems to be a strong repulsion between any two wave fronts. While one might have expected the waves to crash into each other and annihilate themselves, in this system they do not. The two fronts repel each other and will not diffuse into each other, and for a long period of time a region of null precipitation will exist between the two wave fronts (Fig. 4).

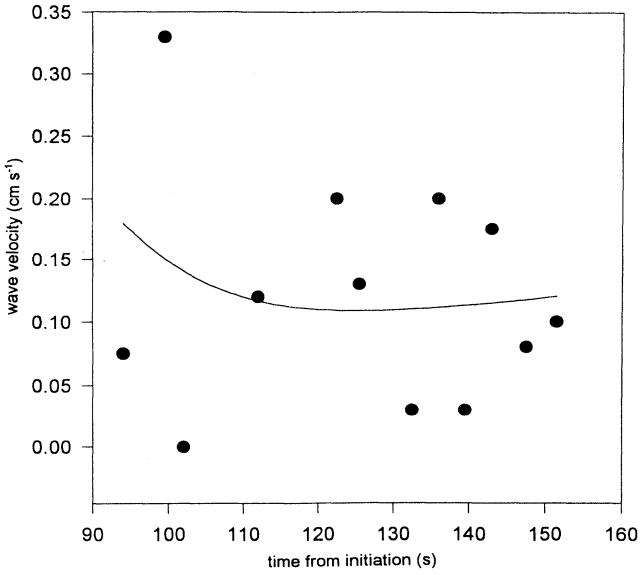

FIG. 2. Velocity variation of the two leading fronts. The solid line presents the leading edge which attains some constant velocity while the velocity of the second wave is oscillatory. The dots represent the velocity of the second front. The solid line was reproducible and is an average from at least ten different experiments. The dots were not as reproducible, but they consistently showed the alternating velocity readings.

Effect of depth

The depth of the solution was important in determining wave velocity, spatiotemporal patterns, and wave

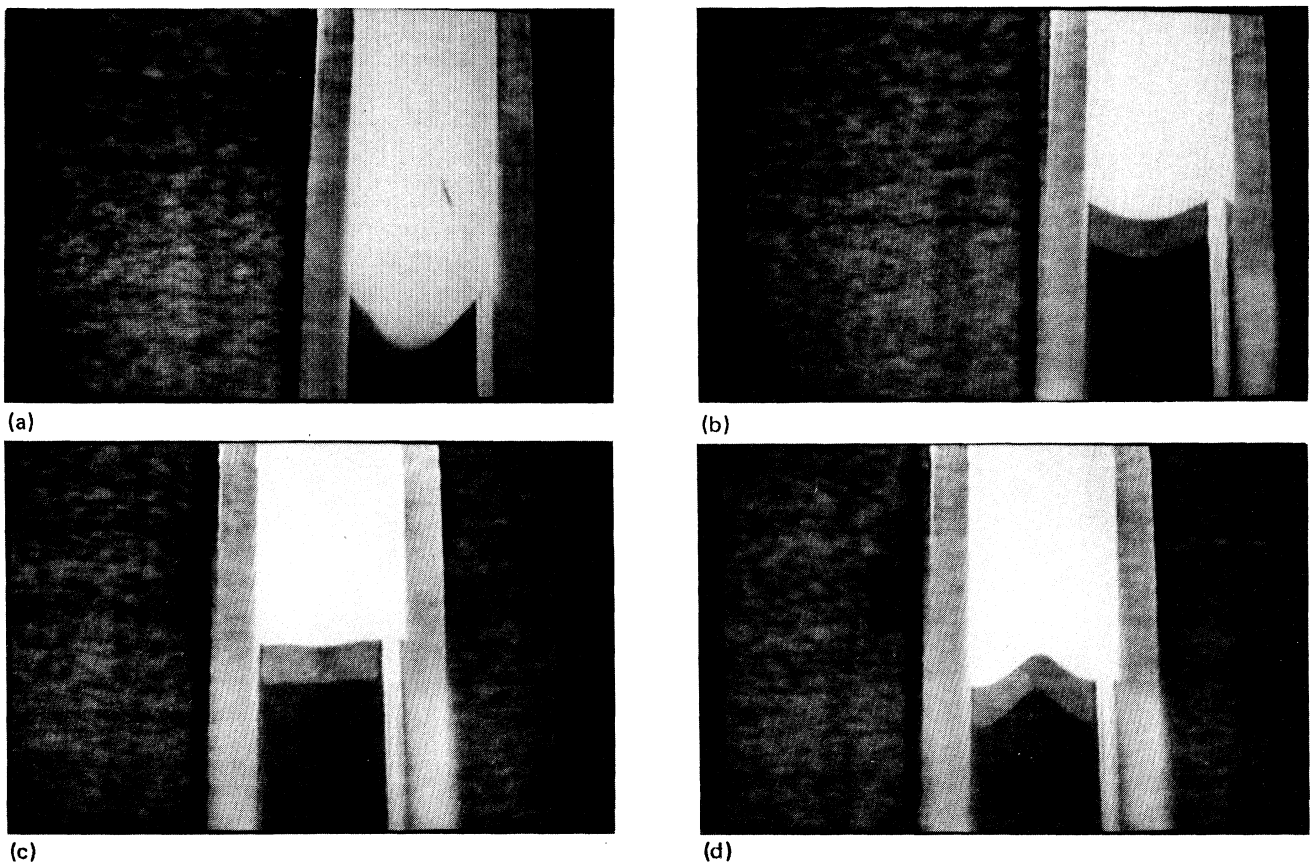

FIG. 3. (a)–(d) The observed wave front bifurcation sequence in a typical big wave. The same sequence has been observed in the Belousov-Zhabotinsky reaction system. See Refs. [28,29]. The width of the reaction vessel is 20 mm.

form. The wave is much faster in deeper layers. In shallow layers the wave starts off fast and quickly decelerates to a slow steady speed as was noted in one of our earlier papers [24]. In deeper solutions, the wave also starts off fast but it accelerates to a higher speed before decelerating to attain a steady speed which is higher than in shallow layers. There was a direct proportionality between the solution depth and the wave velocity. In deep solutions, the wave reaches the end of the reaction vessel (rectangle or triangle) before the "arms" along the vessel walls are fully formed. It thus never experiences the retardation that is brought about by the formation of the "arms." The convective rolls are never clearly defined in deep solutions and back flow is not observed until the wave has decelerated. The periodic precipitation patterns, as well, are quickly annihilated in deep solutions [30]. By using latex beads and barium sulfate precipitation, the velocity profiles in shallow and deep layers are observed to be very different. The shallow layers are easily divided into forward flow and back flow in which the whole solution layer is involved [Fig. 5(a)], but in deep layers only the top part of the solution is involved [Fig. 5(b)]. Thus shallow layers have to deal with sheer (no slip adherence) at the bottom of the vessel which the deeper solutions do not have to. The shallow solutions are very close to a two-dimensional projection of a complex three-dimensional hydrodynamic pattern while the deeper solutions have a finite z-axis component. The absence of clear, robust patterning in deep layers can now be rationalized: barium sulfate precipitating (specific gravity ≈ 4.5) down the solution coupled with double-diffusive convection into the unreacted lower solution will quickly destroy any spatiotemporal organization in the x-y plane.

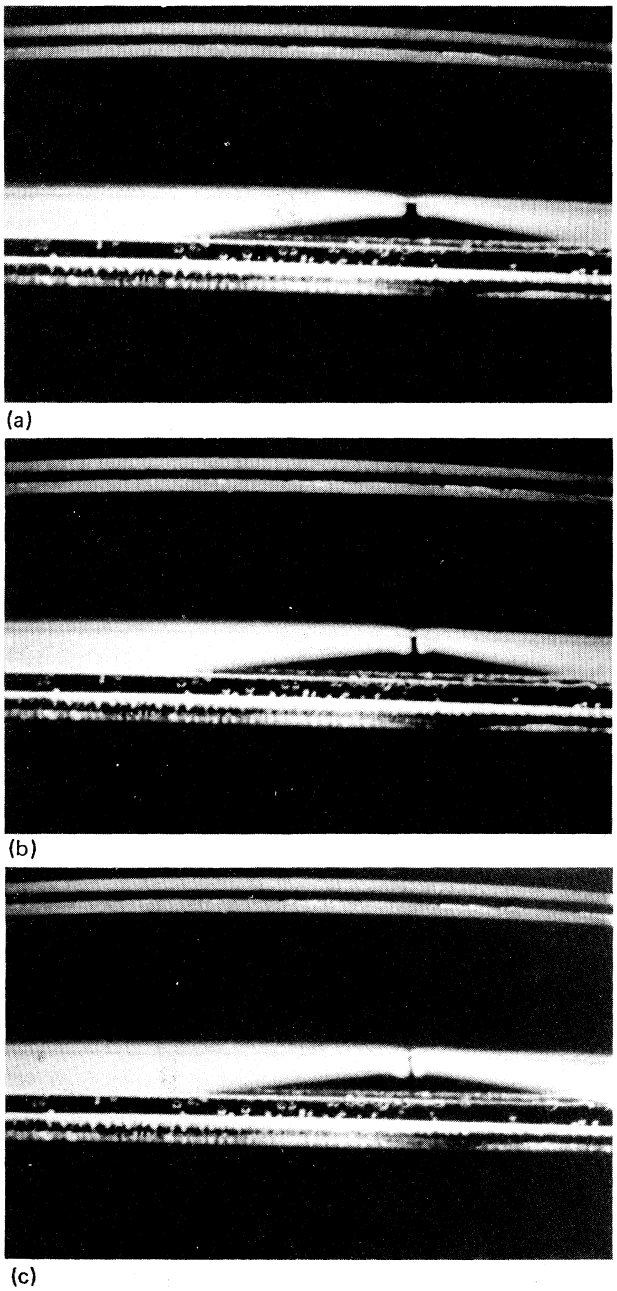

FIG. 4. (a)–(c) The observed repulsion between two wave fronts. The depth of the solution is 10 mm.

Formation of convective torus

For layers with $d \leq 3.4$ mm a convective torus was always evident about 5 s after reaction initiation. The

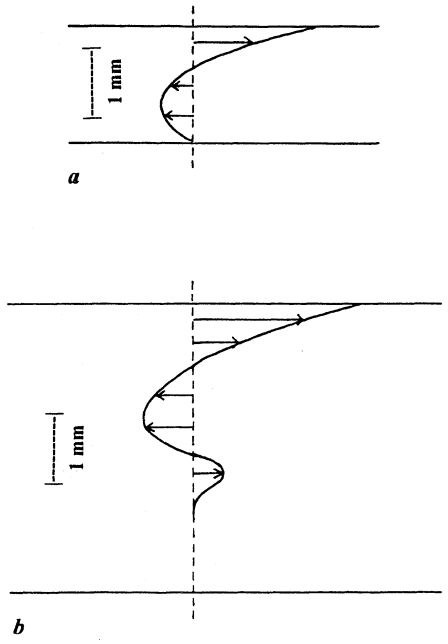

FIG. 5. (a) The observed wave profile in shallow fluid layers. The whole solution layer participates in the overall wave dynamics. The shallow layer is 1.7 mm deep. (b) The profile in deep fluid layers (the depth is 4.3 mm). The solution in the bulk is unaffected by the wave motion above. The bottom layers finally react via a combination of double-diffusive convection, reaction-diffusion mechanisms, and being triggered by the falling $BaSO_4$ precipitate.

torus was formed after the periodic precipitation patterns. The formation of the torus involves the leading front going down the solution, being reflected back by the back flow, and then rising towards the surface behind the leading front to complete the roll. Convective tori are formed only if the wave is initiated from the center of the reaction solution. A torus grows radially outward, but in asymmetric tori, apart from the radial growth, the torus also spun in the x-y plane about the z axis. Figure 6 shows an asymmetric torus which is spinning as it grows. The spin always occurred in the direction having the net resultant thermocapillary force.

The sawtooth effect

As expected from thermocapillary-driven waves, the top of the wave is always ahead of the rest of the wave. We have tracked the shape of the wave with time and this progression is shown in Fig. 7. At the beginning the wave makes a very acute angle θ with the horizontal, with the leading front being well ahead of the bottom layer of the wave. During this time the wave will be traveling at its maximum speed. As time progresses, the angle

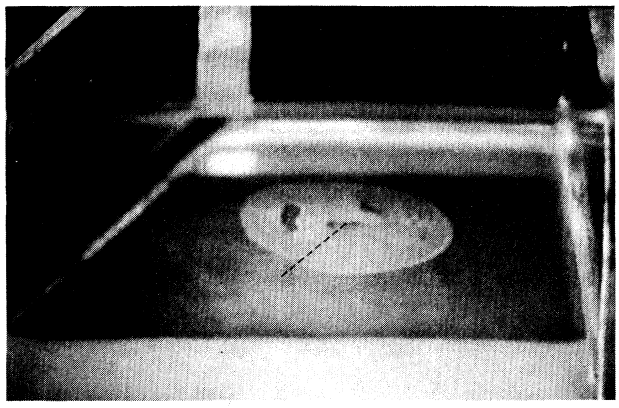

(a)

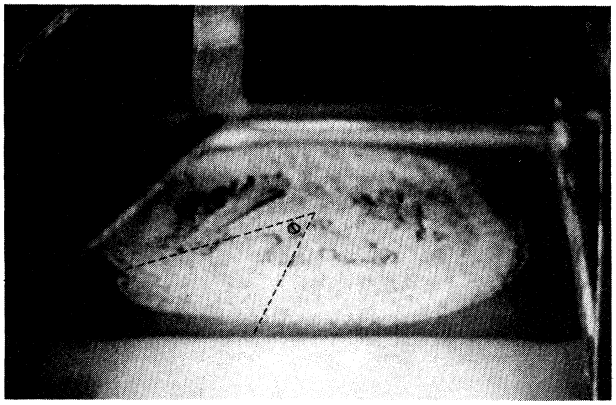

(b)

FIG. 6. (a) and (b) Two pictures of the same torus which show the spinning motion which is the resultant of thermocapillary forces which are unbalanced in the x-y plane. The diameter of the convective torus in (a) is 36 mm, and in (b) it is 64 mm. As it grows, it is also spinning in a clockwise direction. From (a) to (b), it spins by an angle θ.

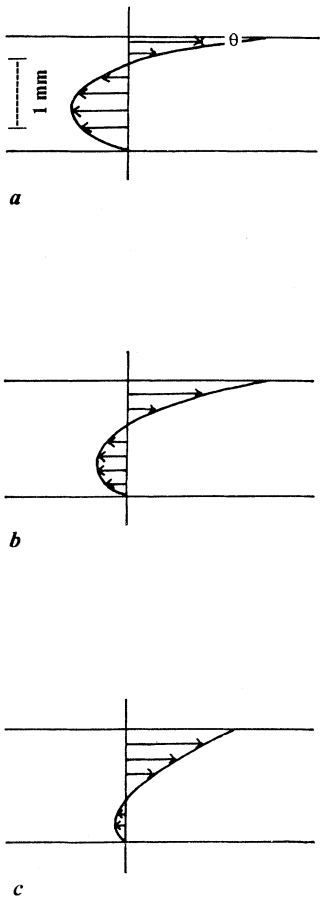

FIG. 7. (a)–(c) Three figures showing the observed shape of the thermocapillary wave with time. As the angle θ increases, the velocity of the front decreases (a) to (c) and the total reaction zone shrinks.

becomes wider as the wave decelerates and the leading front and the trailing back flow come closer together. Some equilibrium angle which is determined by the depth of the solution and amount of heat produced at the wave front [31] is finally achieved. Closer examination of the side view of the wave shows a sawtooth shape (Fig. 8) which can easily be explained by invoking the convective rolls and back flow. The sawteeth are under a constant back flow force and hence are inclined back towards the

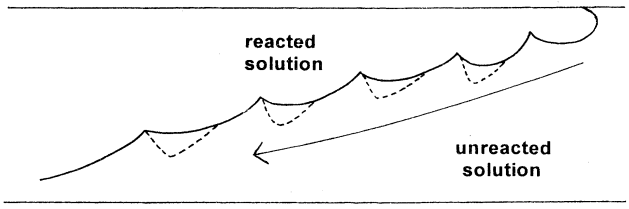

FIG. 8. The shape of the wave in rectangle (B) with solution at a depth of 11.0 mm. The convective rolls are clearly seen along the bottom of the wave front. The bottom of the wave front is under the influence of a back flow, and the wave front oscillates between the solid and dashed lines.

reverse direction of the wave propagation. Each convective roll is demarcated by the edge of a sawtooth.

DISCUSSION

In this work we have managed to assess the effects of buoyancy convection, thermocapillary convection, and reaction-diffusion forces in wave propagation. The hydrothermal waves arising from the Bénard-Marangoni convection appear to be more powerful than expected. All the experimental observations can be rationalized by Bénard-Marangoni effects without resorting to chemical diffusion and reaction kinetics. A very good estimation of the heat generated at the front is the only prerequisite for an understanding of the spatiotemporal patterns and convective rolls.

Wave velocity

Lateral velocity is influenced primarily by the Marangoni effect. From Eq. (2),

$$M \propto \Delta T \ , \tag{9}$$

where ΔT is the temperature change across the surface interface between reacted and unreacted solutions. The driving force comes from the variation in surface tension across the interface. Different fluids have different values for the change in surface tension with temperature, and thus ΔT may not be as good a measure of the Marangoni effect as $\Delta\sigma/\Delta x$. We can write

$$\delta\sigma/\delta x = (\delta\sigma/\delta T)(\delta T/\delta x) \ . \tag{10}$$

$\delta\sigma/\delta T$ is the rate of change of surface tension with temperature *in the linear region* and can easily be experimentally determined for each liquid.

$$\sigma = \sigma_0 - (\delta\sigma/\delta T)(T - T_0) \ , \tag{11}$$

where σ is the surface tension of liquid at temperature T, and σ_0 at T_0. $\delta\sigma/\delta x$ is the required surface tension gradient.

The wave propagation velocity is directly proportional to the heat produced, Q [31]; which in turn is proportional to the initial concentrations of reagents, the enthalpy change for the reaction, and the extent of reaction:

$$Q = f(\Delta H_R, \xi_R, c_i, c_j) \ , \quad Ac_i \geq Bc_j \ , \tag{12}$$

while

$$\Delta T \propto C_P^{-1} \ , \tag{13}$$

where ΔH_R is the enthalpy of the reaction, ξ_R is the extent of reaction, c_i the concentration of the oxidant (oxyhalogen compound), c_j the concentration of the reductant (sulfur compound), and A and B are the stoichiometric coefficients for the reaction. C_P is the *specific* heat capacity of the solution. In dilute aqueous solutions, this can be taken to be the same as the value for pure water.

Our experimental data show that the wave propagation velocity is dependent on the depth of the solution and on the temperature change between the reacted and the unreacted regions of the solution. The wave velocity increased with increase in initial reactant concentrations. Higher reactant concentrations gave a larger temperature jump at the wave front, and subsequently increased the surface tension gradient. This confirmed results from an earlier study [32]. Surface velocity is thus

$$V_s = Cd(\delta\sigma/\delta x) \ . \tag{14}$$

d is the depth of the solution and C is a constant which involves thermal diffusivities and the fluid viscosity. Equation (14) agrees very well with the two-dimensional model of Ezersky *et al.* which predicts that the wave velocities are proportional to d and ΔT when thermocapillary convection dominates [33]. This especially is the case for thin layers where buoyancy effects are negligible.

Energetics of torus formation

Previous studies established a negative partial molar volume change for the series of reactions under study [23]. A front with the hot reacted solution on top and cold unreacted solution below will be unstable to small perturbations as any deformation of the interface will result in the formation of fingers of reacted solution going down into the unreacted region [34,35]. Convective tori are formed when the wave decelerates and the thermocapillary force goes down. At this stage any finger that goes down the solution will be swept backwards by the back flow that is resident at the bottom of the solution. This scenario is sketched in Fig. 9. The torus encircles a region of unreacted solution which leads to the spatiotemporal patterns later observed.

CONCLUSION

This work clearly establishes the dominance of the Marangoni effect in propagating convective fronts. The important parameter is the amount of heat generated at the reaction front. Heat diffusion is 100× more efficient [23] than diffusion of chemical reactants, and hence with high enough heat generation the standard reaction-

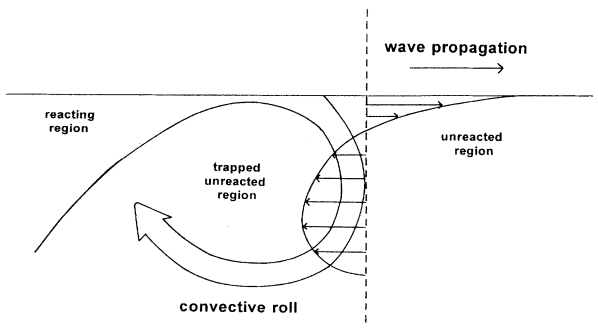

FIG. 9. A schematic diagram which shows the mechanism of torus formation. Any finger which falls to the bottom of the solution layer will be quickly swept back by the resident back flow in that region. Further reaction in the solution in the finger region will produce enough heat to allow the finger to rise and complete the convective roll.

diffusion mechanisms are insignificant except in situations in which $\delta\sigma/\delta T$ is positive. In this case the Marangoni effect will be in the direction opposite to the reaction-diffusion propagation in autocatalytic convective fronts. A combination of the Marangoni effect with Rayleigh-Bénard convection gives the convective rolls. As long as the reaction front is hotter than the unreacted solution, the reacted solution will be light enough to slide over the unreacted solution, even if the system has a negative partial molar volume change. Since reactions are not run at isothermal conditions, the cooling of the reacted solution then contributes to the exotic dynamics observed in these chemical systems. Marangoni convection is a surface flow (roller conveyor condition), and is at its maximum at the boundary layer [15]. With the standard no-slip (adherence) condition, the stream velocity drops off to zero at wall boundaries. The Marangoni effect will only exist if the upper surface is free and open to the atmosphere.

Surprisingly, results obtained in this report were also obtained in a system of shallow layers of acetone subjected to a horizontal temperature gradient [36]. This situation is similar to our chemical system since the wave front approximates to the hot end of the layer [37]. The only difference is a shrinking horizontal coordinate in the chemical front propagation. The role of standard reaction-diffusion models as governed by Eq. (1) is minimal in a convective system with large heat generation at the wave front.

ACKNOWLEDGMENTS

We acknowledge helpful discussions with Cordelia Chinake and Marcus Hauser. We are grateful to the University of Natal for giving leave of absence and a sabbatical grant to one of us (B.S.M.). This work was supported by a NSF-EPSCoR grant.

[1] M. Orbán, J. Am. Chem. Soc. **102**, 4311 (1980).
[2] M. C. Cross and P. C. Hohenberg, Rev. Mod. Phys. **65**, 851 (1993).
[3] A. M. Turing, Trans. R. Soc. London Ser. B **327**, 37 (1952).
[4] G. Kshirsagar, Z. Noszticzius, W. D. McCormick, and H. L. Swinney, Physica D **49**, 5 (1991).
[5] N. Kreisberg, W. D. McCormick, and H. L. Swinney, J. Chem. Phys. **91**, 6532 (1989).
[6] M. Diewald and H. R. Brand, Chem. Phys. Lett. **216**, 566 (1993).
[7] M. Lucke, M. Mihelicic, and B. Kowalski, Phys. Rev. A **35**, 4001 (1987).
[8] H. Bénard, Rev. Gen. Sci. Pures Appl. **11**, 1261 (1990).
[9] Lord Rayleigh, Philos. Mag. **32**, 529 (1916).
[10] J. R. A. Pearson, J. Fluid Mech. **4**, 489 (1958).
[11] K. A. Smith, J. Fluid Mech. **24**, 401 (1966).
[12] D. A. Nield, J. Fluid Mech. **19**, 341 (1964).
[13] J. Metzger and D. Schwabe, Physicochem. Hydrodyn. **10**, 263 (1988).
[14] L. E. Scriven and C. V. Sternling, J. Fluid Mech. **19**, 321 (1965).
[15] J. A. Szymczyk, Can. J. Chem. Eng. **69**, 1271 (1991).
[16] M.-I. Char and K.-T. Chiang, J. Phys. D: Appl. Phys. **27**, 748 (1994).
[17] M. K. Smith and S. H. Davis, J. Fluid Mech. **132**, 145 (1983).
[18] C. R. Chinake and R. H. Simoyi, J. Phys. Chem. **97**, 11 569 (1993).
[19] I. R. Epstein, K. Kustin, and R. H. Simoyi, J. Phys. Chem. **96**, 5852 (1992).
[20] G. Peintler, I. Nagypal, and I. R. Epstein, J. Phys. Chem. **94**, 2954 (1990).
[21] G. Rábai and M. Orbán, J. Phys. Chem. **97**, 5935 (1993).
[22] H. Taube and H. Dodgen, J. Am. Chem. Soc. **71**, 3330 (1949).
[23] C. R. Chinake and R. H. Simoyi, J. Phys. Chem. **98**, 4012 (1994).
[24] M. J. B. Hauser and R. H. Simoyi, Phys. Lett. A **191**, 31 (1994).
[25] A. Indelli, J. Phys. Chem. **68**, 3027 (1964).
[26] M. J. B. Hauser and R. H. Simoyi, Chem. Phys. Lett. **227**, 593 (1994).
[27] This was first observed in these chemical systems for reactions run in a Petri dish. In this round vessel, the null precipitation ring was much larger. See Ref. [24].
[28] This was also observed in an unrelated chemical system. See H. Miike, H. Yamamoto, S. Kai, and S. C. Muller, Phys. Rev. E **48**, 1627 (1993).
[29] S. Kai and H. Miike, Physica A **204**, 346 (1994).
[30] M. J. B. Hauser and R. H. Simoyi (unpublished results).
[31] Amount of heat generated is proportional to the enthalpy change of the reaction, which is an extensive property of the system. Higher reagent concentrations produce a sharper thermal gradient at the wave front.
[32] R. H. Simoyi, J. Masere, C. Muzimbaranda, M. Manyonda, and S. Dube, Int. J. Chem. Kinet. **23**, 419 (1990).
[33] A. B. Ezersky, A. Garcimartin, J. Burguete, H. L. Mancini, and C. Perez-Garcia, Phys. Rev. E **47**, 1126 (1993).
[34] J. S. Turner, Annu. Rev. Fluid Mech. **17**, 11 (1985).
[35] H. E. Huppert and J. S. Turner, J. Fluid Mech. **106**, 299 (1981).
[36] D. Villers and J. K. Platten, J. Fluid Mech. **234**, 487 (1992).
[37] Spatiotemporal and monocellular steady states were obtained in Ref. [35] in a system with a fixed cavity length. In our chemically driven system the cavity length is constantly changing as the reaction front encroaches towards the other end of the reaction vessel.

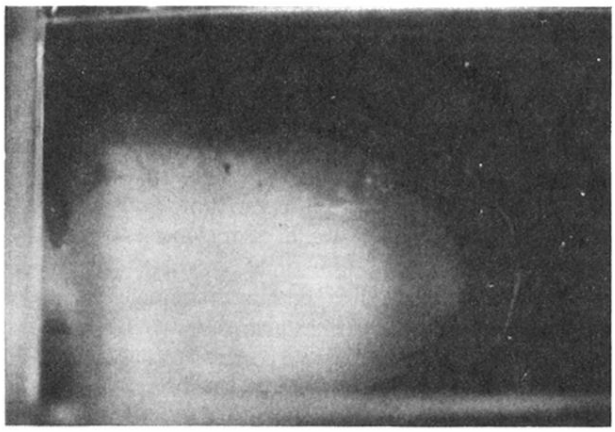

(a)

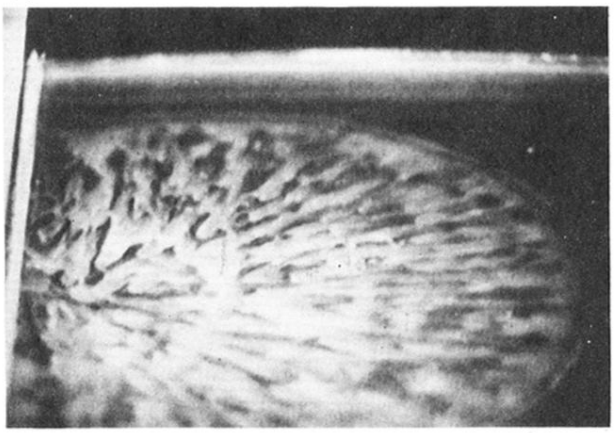

(b)

FIG. 1. (a) A typical wave observed in a large vessel (with no interference from the walls). Leading edge is clearly marked by faint precipitation; the next region has inhomogeneous $BaSO_4$ precipitate distribution. The width of the leading edge in this figure is 12 mm. (b) Close-up of the leading front which is separated from the rest of the wave by an annulus of null precipitation. The annulus shown here is 3 mm wide.

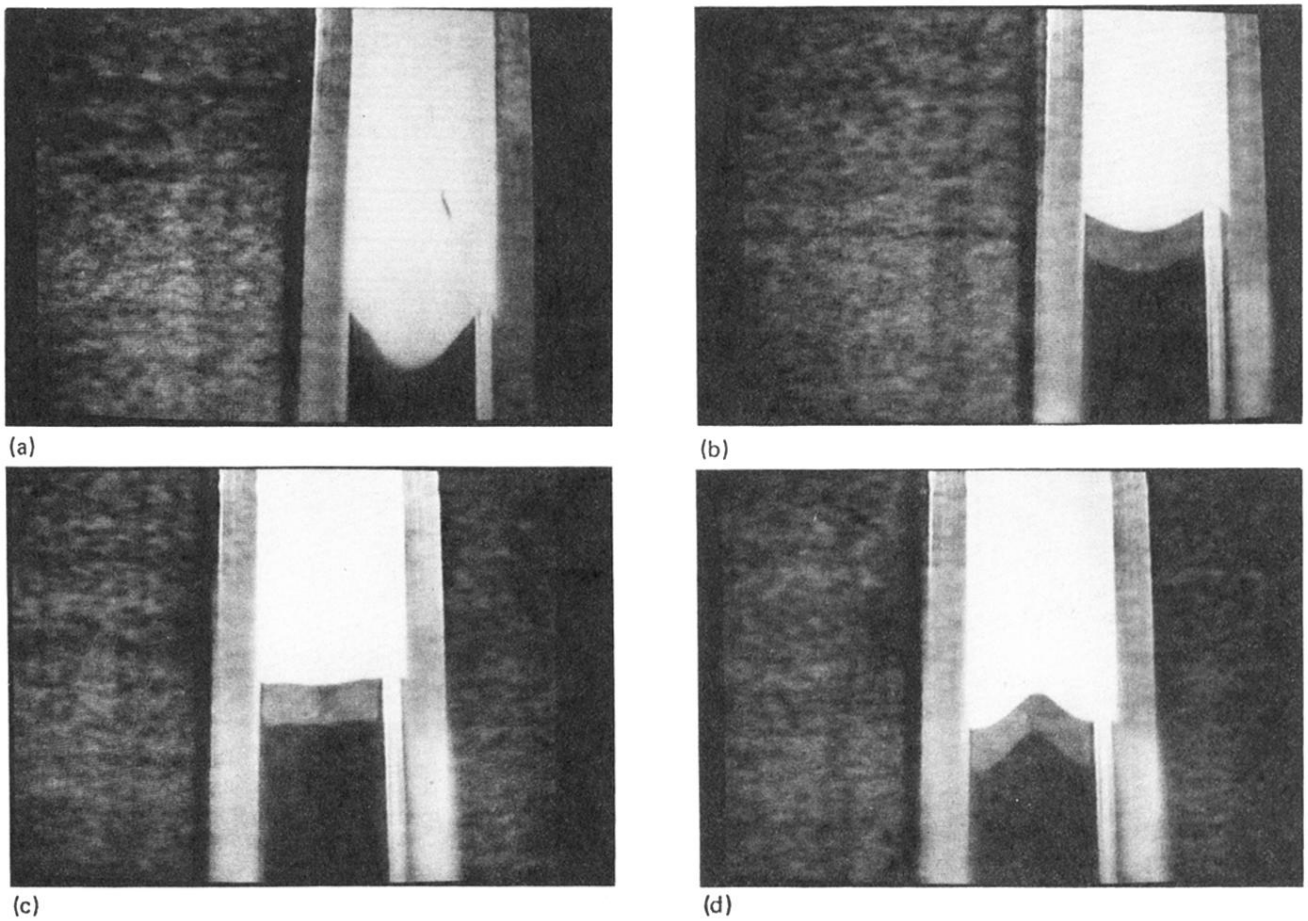

FIG. 3. (a)–(d) The observed wave front bifurcation sequence in a typical big wave. The same sequence has been observed in the Belousov-Zhabotinsky reaction system. See Refs. [28,29]. The width of the reaction vessel is 20 mm.

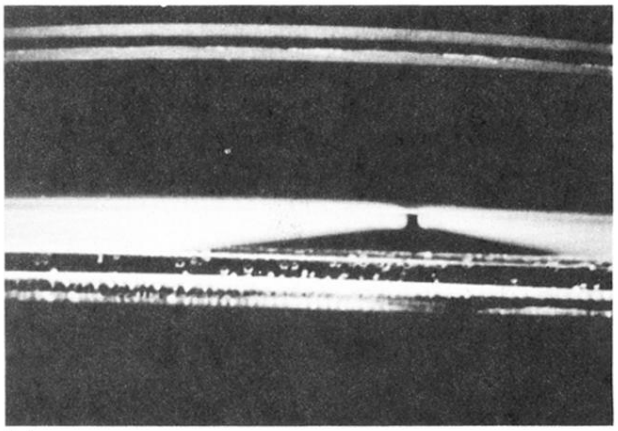

(a)

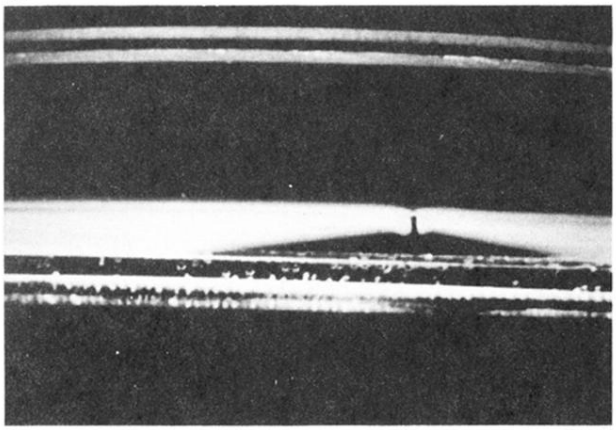

(b)

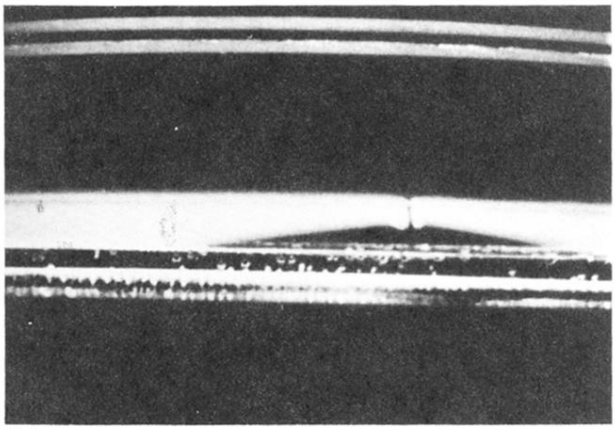

(c)

FIG. 4. (a)–(c) The observed repulsion between two wave fronts. The depth of the solution is 10 mm.

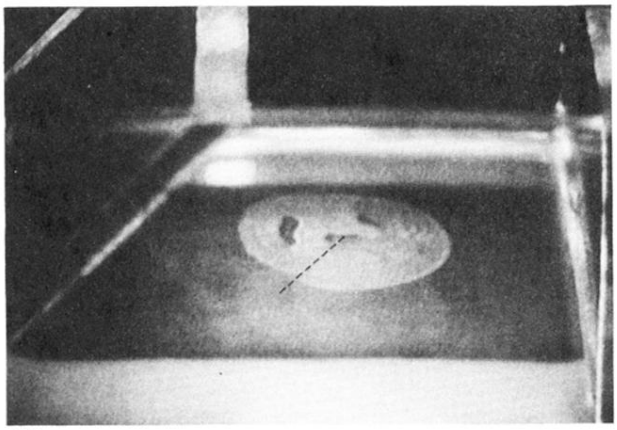

(a)

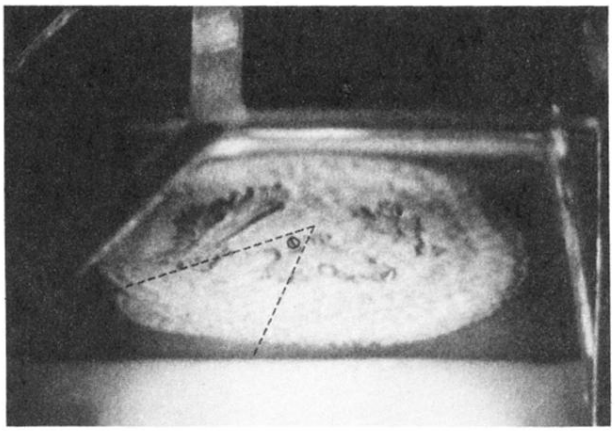

(b)

FIG. 6. (a) and (b) Two pictures of the same torus which show the spinning motion which is the resultant of thermocapillary forces which are unbalanced in the x-y plane. The diameter of the convective torus in (a) is 36 mm, and in (b) it is 64 mm. As it grows, it is also spinning in a clockwise direction. From (a) to (b), it spins by an angle θ.